RESEARCH ARTICLE - APPLIED GEOPHYSICS

Estimation of water saturation based on optimized models in tight gas sandstone reservoirs: a case study of Triassic Xujiahe Formation in northwestern Sichuan Basin

Xiaoyong Xia[1] · Bing Han[1,2] · Bing Xie[1] · Qiang Lai[1] · Yuexiang Wang[1] · Shaowu Zhu[3]

© The Author(s) under exclusive licence to Institute of Geophysics, Polish Academy of Sciences 2024

Abstract

Water saturation estimation faced a great challenge in tight gas sandstone reservoirs because of the effect of pore structure and strong heterogeneity. The classic Archie's equation cannot be always well used. To quantify the effect of pore structure to rock resistivity in tight gas sandstones, taking Triassic Xujiahe Formation of northwestern Sichuan Basin as an example, 35 core samples were recovered and applied for resistivity experiments in laboratory under the simulated formation temperature and pressure environment, and 18 of them were simultaneously applied for nuclear magnetic resonance (NMR) and high-pressure mercury injection experimental measurements. Relationships between pore structure and resistivity parameters were analyzed. The results clearly illustrated that cementation exponent (m) and saturation exponent (n) were heavily affected by pore structure. Rocks with superior pore structure contained relatively higher cementation exponent and lower saturation exponent, and vice versa. Afterward, we raised a parameter of pore size index, which was defined as the ratio of macropore and micro-pore percentage contents, to characterize rock pore structure, and established a model to calculate optimal saturation exponent from NMR data. Meanwhile, cementation exponent prediction model was also raised by combining with porosity and irreducible water saturation (S_{wirr}). Combining with calculated cementation exponent and saturation exponent, we optimized the Archie's equation to predict water saturation in our target tight gas sands. Field examples illustrated that the predicted cementation exponent and saturation exponent matched well with core-derived results. The absolute errors between predicted cementation exponent and saturation exponent with core-derived results were lower than 0.05 and 0.07, separately. By using optimized Archie's equation, water saturations were precisely predicted from well logging data in our target tight gas sandstone reservoirs; whereas, the classic Archie's equation underestimated formation water saturation.

Keywords Water saturation · NMR measurements · Tight gas sandstone · Pore structure · Optimized saturation models

---

Edited by Prof. Jadwiga Anna Jarzyna (ASSOCIATE EDITOR) / Prof. Ali Gholami (CO-EDITOR-IN-CHIEF).

✉ Xiaoyong Xia
565042074@qq.com

Bing Han
han.bing@petrochina.com.cn

[1] Research Institute of Exploration and Development, Southwest Oil and Gas Field Company, PetroChina, Chengdu, Sichuan, China

[2] Present Address: Research Institute of Exploration and Development, Southwest Oil and Gas Field Company, PetroChina, Chengdu, Sichuan, China

[3] Southwest Petroleum Logging Company, China Petroleum Logging Co. Ltd, Chongqing, China

Introduction

Water saturation was defined as the ration of pore volume that occupied by water with total rock pore volume (Picket 1966). It was an important input parameter in formation evaluation, pore fluid identification and reserve estimation (Ferraris and Carnegie 2005; Liu and Hu 2010). Hence, accurately calculating water saturation has always been a major goal pursued by petrophysicists (Xiao et al. 2013, 2015). In conventional reservoirs, saturation evaluation problem had been overcome since the Archie's equation was first raised in 1942 (Archie 1942). The pore structure, which was defined as pore size and connectivity, were relatively simple in such type of formation, and relationships between porosity and formation factor, water saturation versus resistivity index can be well expressed by power function (Guo

et al. 2023; Gupta and Kamal 2023). The Archie's equation had been widely used for a long time. However, the limitations and applicability of Archie's equation were increasingly being revealed after complicated reservoirs were recovered, e.g., low resistivity contrast hydrocarbon-bearing reservoirs, low permeability to tight reservoirs (Mahmood et al. 2023; Qian et al. 2023). To improve water saturation prediction accuracy, many models had been proposed since 1950s (Simandoux 1963; Waxman and Smits 1968; Poupon and Leveaux 1971; Waxman and Thomas 1974; Clavier et al. 1984; Rasmus 1985; Givens 1987; Givens and Schmidt 1988; Song et al. 1995; Mao et al. 1999; Mo et al. 2001; Liu et al. 2009; Zhang et al. 2010; Li et al. 2012, 2020; Sarihi and Vargas-Murillo 2015; Hou et al. 2023). In low-resistivity contrast hydrocarbon-bearing reservoirs, several popular models were proposed to calculate water saturation after the genetic mechanism that decreased formation resistivity was considered. The Simandoux's equation and Indonesia formula were used to calculate water saturation in shaly-rich sandstone reservoirs (Simandoux 1963; Poupon and Leveaux 1971). The Waxman-Smits' equation and dual-water model were used in formations with strong additional conduction that caused by cation exchange (Waxman and Smits 1968; Waxman and Thomas 2007; Clavier et al. 1984). The Givens' model was available in low resistivity contrast formation that caused by metal mineral conduction, and these metal minerals were contained in rock matrix (Givens 1987; Givens and Schmidt 1988). These models had played an irreplaceable role in water saturation prediction, and were still in use in clastic reservoirs at this stage. However, they were only usable in low resistivity contrast hydrocarbon-bearing formations. In tight sandstone reservoirs, the main factor that led to complex conductivity was pore structure (Xie et al. 2023). The other factors, e.g., high shale content, cation additional conduction, and the presence of conductive matrix, can be ignored. In recent years, the digital core technique has been widely used to simulate rock electrical properties (Liu et al. 2009; Walsh and Vogler 2020; Ammar 2021; Hou et al. 2023). Based on the digital core, the resistivity index that corresponded to low water saturation can be simulated to restore the complete conductivity. Digital core technique was well used in rocks with complicated pore structure, especially in double porosity media, e.g., volcanics and carbonatite (Ahmed et al. 2018). This technique was only used in laboratory to simulate rock electrical properties, it cannot be directly used in field applications at present.

To precisely calculate water saturation in field applications in tight sandstone reservoirs, many scholars raised novel models, such as three-water model, parallel conduction model (Mo et al. 2001; Zhang et al. 2010; Umezawa et al. 2021). Although these models were usable in tight sandstones, too many input parameters were involved, and difficult to be acquired. For example, the volumes of clay

water and capillary moisture cannot be estimated from well logging except for nuclear magnetic resonance (NMR) logging (Coates et al. 2000; Dunn et al. 2002). To calculate water saturation in formation with complicated pore structure, many optimized models were raised. Liu et al. (2012) and Xiao et al. (2013) pointed out that pore structure heavily affected the conductivity in tight sandstone reservoirs, and derived a theoretical model to calculate cementation exponent from porosity. Meanwhile, Xiao et al. (2013) also raised a statistical model to predict saturation exponent from NMR logging to optimize the Archie's equation. These proposed models had been verified to be usable in certain reservoirs (Gao et al. 2023; Li et al. 2023). However, the wide applicability was questionable. The conductivity in tight sandstone was dominantly determined by pore structure; whereas, cementation exponent was only predicted from total porosity (Mao et al. 1997; Xiao et al. 2013). In fact, porosity cannot be simply used to fully reflect rock pore structure. Many rocks contained high porosity but low permeability due to the contribution of poor pore connectivity (Mao et al. 2013). This made the raised model by Xiao et al. (2013) unable to work well in tight sandstone reservoirs. To establish a reasonable model that can be well used to predict water saturation, the pore structure should be first considered.

The purpose of this study was to establish models to optimize cementation exponent and saturation exponent after poor pore structure was considered in tight sandstone reservoirs. To establish these models, the Triassic Xujiahe Formation, which was located at the Northwestern Sichuan Basin, was chosen as an example. In these models, the change of cementation exponent and saturation exponent raised by pore structure were quantified, and models of predicting these two parameters were established to optimize Archie's equation. Application of optimized Archie's equation in our target tight gas sandstones illustrated that the calculated water saturation matched well with the core-derived results; whereas, the predicted water saturation was underestimated based on classic Archie's equation once fixed cementation exponent and saturation exponent were directly used.

Effect of pore structure to electrical properties in tight sandstone reservoirs

Rock resistivity properties in our target tight sandstone reservoirs

Generally, the electrical properties of rocks can be expressed by using the Archie's equation (Archie 1942). The Archie's equation bridged the gap between porosity, resistivity, and water saturation, and can be expressed as follows:

$$FF = \frac{R_0}{R_w} = \frac{a}{\varphi^m}, \tag{1}$$

$$Ir = \frac{R_t}{R_0} = \frac{1}{S_w^n}, \tag{2}$$

where FF was the formation factor, and Ir was the resistivity index, they were all dimensionless. φ was the porosity in fraction, and S_w was the water saturation in fraction. R_0 was the rock resistivity under fully water saturation, R_t was the rock resistivity under hydrocarbon saturated, and R_w was the formation water resistivity. The unit of them was Ω.m. a was a coefficient that related to lithology, m was the cementation exponent, and n was the saturation exponent. They were dimensionless. a, m and n were collectively referred to as rock resistivity parameters.

The Archie's equation can be expressed by the crossplots of porosity and formation factor, water saturation versus resistivity index after sufficient core samples were drilled and applied for resistivity experiments in laboratory. Once rocks contained relative simply pore structure, crossplots of porosity and formation factor, water saturation versus resistivity index were regular, and fixed cementation exponent and saturation exponent can be acquired. However, in formations with complicated pore structure, simple power function cannot be used to express these relationships.

In our target Triassic Xujiahe Formation, 35 core samples were drilled for resistivity experiments in laboratory under simulated formation temperature and pressure environment, and crossplots of φ and FF, S_w versus Ir are acquired and displayed in Fig. 1. It notably illustrated that the relationships of φ and FF, S_w versus Ir cannot be simply expressed

by power function, the trend lines were crooked. Although the correlation coefficient between S_w and Ir was high, the trendline was tortuous when S_w was higher than 75.0%. In addition, based on Fig. 1b, we could conclude that the resistivity index was equaled to 0.8969 when core samples were fully saturated with water (S_w was equaled to 1.0). This was not in line with theory and practice. Hence, no fixed cementation exponent and saturation exponent can be acquired from these core samples. If we compulsively use fixed parameters, unreliable water saturation would be calculated.

Effect of pore structure to rock resistivity properties

To analyze the reason that caused the relationships between φ and FF, S_w versus Ir exhibited as non-Archie's equation, we selected 18 out of 35 core samples to apply for nuclear magnetic resonance (NMR) and high-pressure mercury injection (HPMI) experiments in laboratory. Table 1 lists the experimental results of resistivity, NMR and HPMI for these 18 core samples. Porosity of these core samples only ranged from 4.48 to 12.29%, and permeability distributed from 0.023 to 0.298 mD. The selected 18 cores were representative, they can be used to reflect physical properties of our target Triassic Xujiahe Formation (Fig. 2c and d). Figure 2a and b indicates that our target tight sandstone reservoirs exhibited poor pore structure and weak rock physical properties, and thus weak relationship between core-derived porosity and permeability. This generated that the cementation exponent changed from 1.90 to 2.18, and the saturation exponent ranged from 1.78 to 2.14.
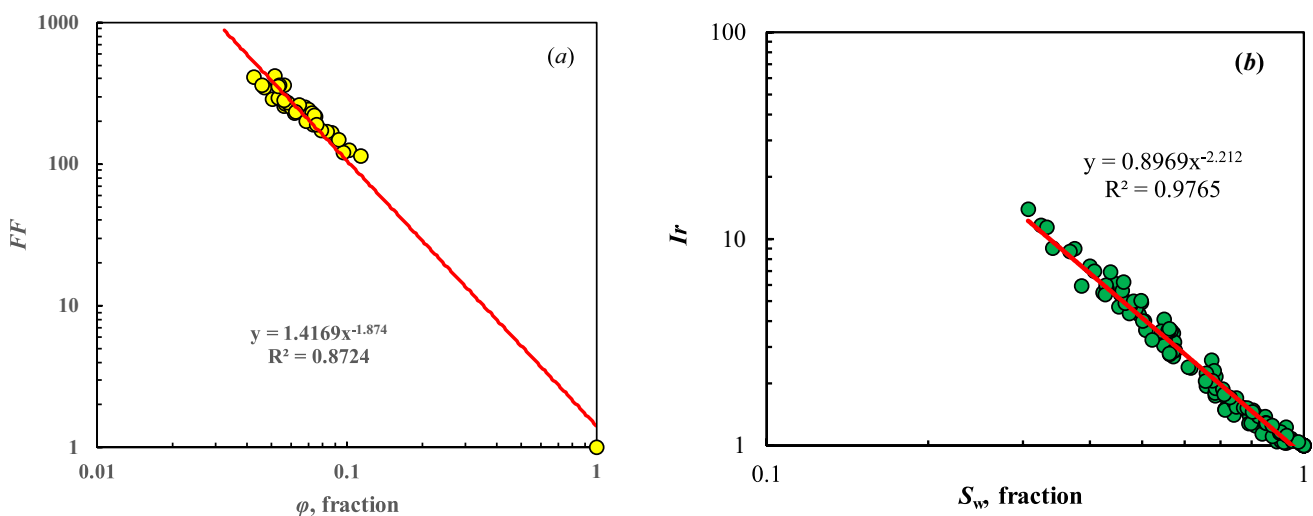

Fig. 1 Crossplots of porosity versus formation factor (**a**), water saturation versus resistivity index (**b**) in our target tight sandstone reservoirs of Triassic Xujiahe Formation in northwestern Sichuan Basin

Table 1 Experimental results of resistivity, NMR and HPMI for 18 core samples that drilled from Triassic Xujiahe Formation in northwestern Sichuan Basin

| Well name	Core No	Depth (m)	Porosity (%)	Permeability (mD)	Cementation exponent	Saturation exponent	T_2 cutoff (ms)	S_{wirr} (%)	T_{2lm} (ms)	Threshold pressure (Mpa)	Maximal pore throat radius (μm)	Average pore throat radius (μm)	Median mercury injection pressure (Mpa)
Well A	1	3124.29	5.00	0.035	1.90	1.83	9.88	53.02	10.19	4.12	0.18	0.04	0.01
Well A	2	/	5.20	0.056	1.94	1.86	11.22	50.01	12.57	1.37	0.54	0.14	0.03
Well A	3	3128.19	5.60	0.056	1.93	1.89	12.12	51.29	13.11	0.68	1.09	0.22	0.10
Well A	4	3129.07	6.15	0.058	1.97	1.88	12.29	50.15	14.41	0.68	1.08	0.20	0.06
Well A	5	3131.50	5.88	0.045	1.94	1.98	7.60	53.05	8.53	1.36	0.54	0.13	0.02
Well A	6	3133.55	5.06	0.029	2.03	2.14	11.19	62.88	7.77	1.36	0.54	0.14	0.03
Well A	7	3140.88	4.48	0.023	1.90	1.95	14.53	65.04	8.79	0.67	1.09	0.18	0.04
Well A	8	3194.78	4.75	0.036	1.91	1.96	8.14	55.23	7.74	1.37	0.54	0.12	0.04
Well A	9	3198.23	7.29	0.164	2.06	1.81	22.60	44.02	29.26	0.68	1.09	0.20	0.06
Well A	10	3198.96	7.73	0.160	2.07	1.82	15.84	36.29	22.88	0.68	1.09	0.15	0.06
Well A	11	3199.72	7.85	0.105	2.02	1.87	18.57	40.19	26.72	0.68	1.09	0.17	0.09
Well B	12	3540.39	10.93	0.116	2.12	1.82	6.00	27.33	13.94	0.68	1.09	0.17	0.09
Well B	13	3543.06	10.32	0.060	2.05	1.78	4.80	27.59	11.24	0.68	1.08	0.18	0.06
Well B	14	3546.61	9.38	0.061	2.09	1.84	4.37	31.42	9.05	0.47	1.57	0.33	0.16
Well B	15	3553.94	12.29	0.298	2.18	1.79	8.06	25.51	23.97	0.68	1.09	0.18	0.18
Well B	16	3555.53	8.07	0.034	2.07	1.86	4.96	42.02	8.25	0.68	1.09	0.18	0.09
Well B	17	3561.34	9.77	0.147	2.10	1.80	8.13	29.02	17.78	0.68	1.08	0.20	0.21
Well B	18	3567.67	8.83	0.133	2.06	1.80	6.10	30.07	11.57	0.47	1.57	0.35	0.27
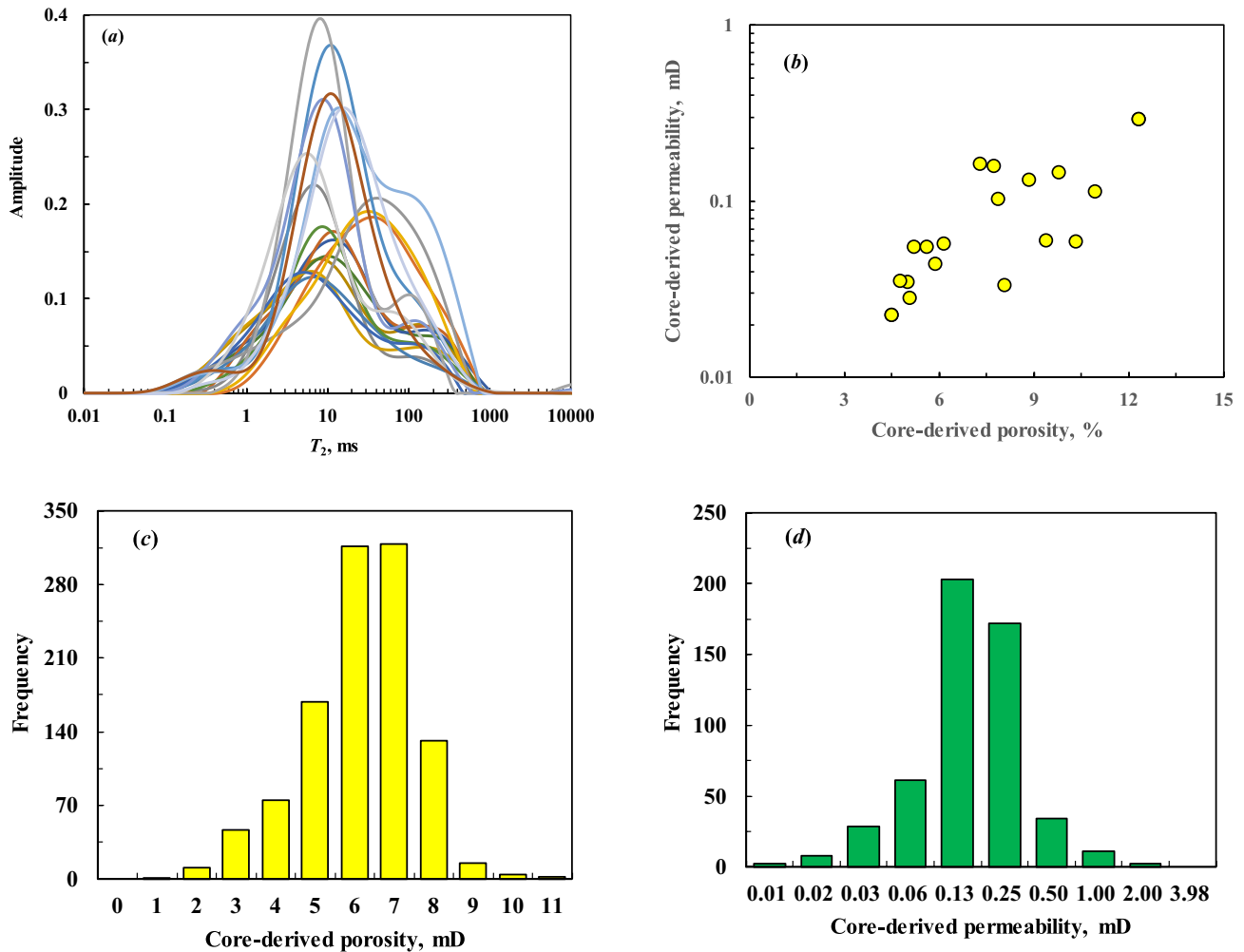
Fig. 2 NMR T_2 distributions (**a**), crossplot of core-derived porosity and permeability (**b**) for 18 core samples with resistivity experiments. Statistical histogram of porosity (**c**), and permeability (**d**) for all 528 core samples in Triassic Xujiahe Formation

Relationship between pore structure and cementation exponent

Figure 3a displays the crossplot of porosity versus formation factor for two typical core samples. These two core samples contained similar porosity and permeability. However, their cementation exponent and saturation exponent were absolutely different. Rock resistivity parameters of core no. 1 were observably lower than that of core no. 6. Based on the macroscopic physical parameters, this difference cannot be clearly interpreted. However, the micro-pore structure can well reflect this variety of cementation exponent and saturation exponent. Although the pore structure of these two core samples was poor, the movable pore volume of no. 1 core sample was relatively higher.

Figure 3b and c displays the corresponding NMR T_2 spectra and HPMI curves for these two core samples. The pore structure of no. 1 core sample was much superior. The pore

space consisted of large pores that flow freely and small pores that cannot flow, and the pore volume of free fluid reached to 46.98%. However, the pore volume of no. 6 core sample dominated by irreducible water, and the irreducible water saturation was higher to 62.88%. Meanwhile, the median mercury injection pressure of no. 1 core sample was half that of no. 6 core sample.

To quantitatively reflect the effect of pore structure to cementation exponent, crossplots of pore structure parameters with cementation exponent for these 18 core samples are analyzed and displayed in Figure 4a–f, separately. Some regularity can be concluded as:

a) Cementation exponents were various but not a fixed value in tight sandstone reservoirs, a uniform cementation exponent cannot be acquired to calculate water saturation by using Archie's equation.
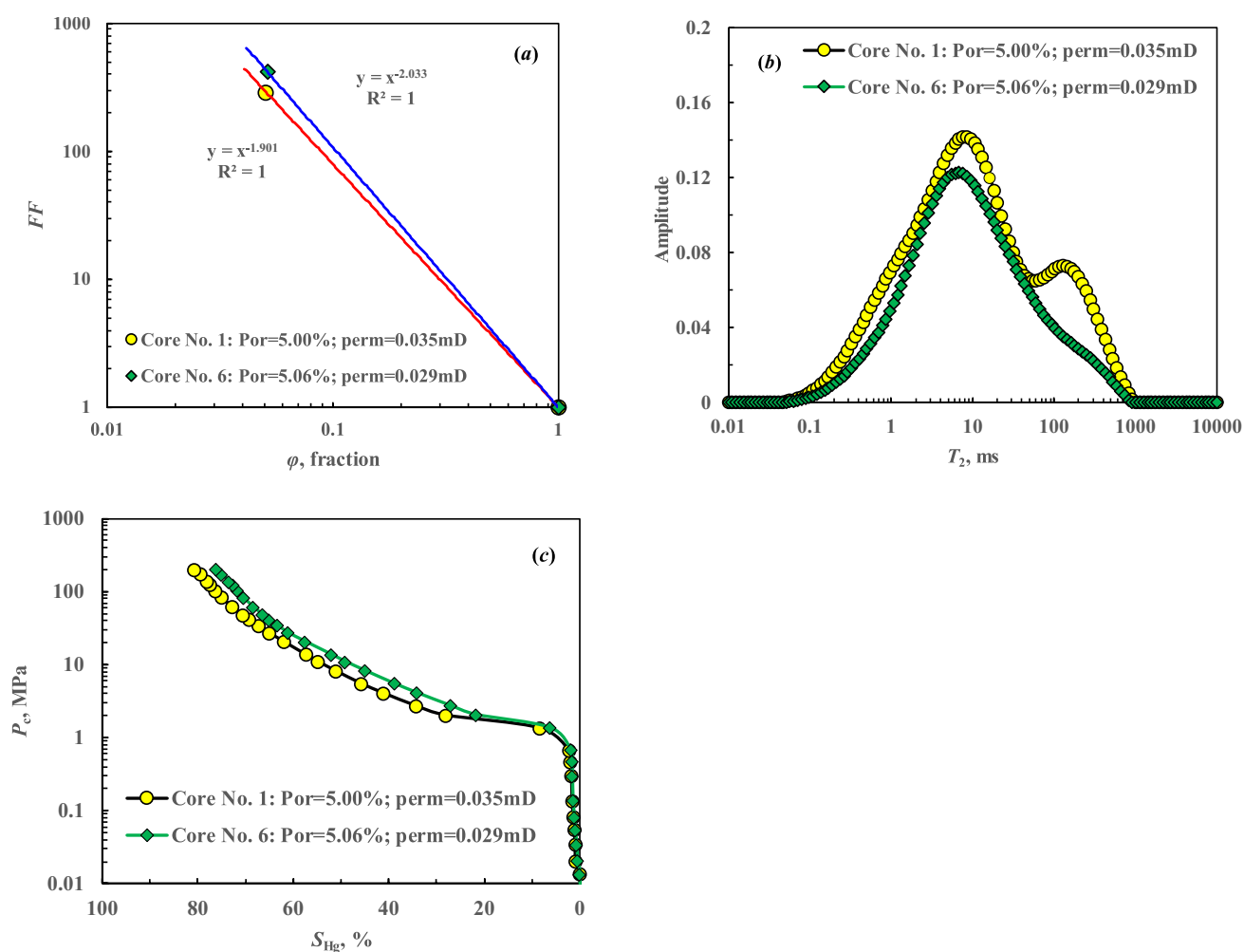
Fig. 3 Crossplot of porosity versus formation factor (**a**), NMR T_2 distributions (**b**) and HPMI curves (**c**) for two typical core samples with different cementation exponent and saturation exponent

b) Cementation exponent was relevant with rock pore structure. The better the pore structure, the higher the cementation exponent.

c) Parameters that heavily associated with cementation exponent were porosity and irreducible water saturation (S_{wirr}, reflecting the relative content of small pores). Although other parameters, e.g., logarithmic mean of transverse relaxation time (T_{2lm}), T_2 cutoff, the average pore throat radius (R_m), and median mercury injection pressure (P50), also positively related to cementation exponent, the correlation coefficients were low enough to be ignored. In addition, these parameters cannot be directly acquired. Pseudo-capillary pressure curves need to be first synthesized from NMR logging, some additional errors were introduced (Xiao et al. 2016).

Relationship between pore structure and saturation exponent

In Figure 5a, we displayed the crossplot of water saturation versus resistivity index for three typical core samples, and the saturation exponents of these core samples changed from 1.786 to 2.137. In Figure 5b and c, we displayed the corresponding NMR T_2 distributions and HPMI curves. Comparisons of these three figures illustrated that saturation exponent was inversely proportional to pore structure. From no. 6 to no. 15 core sample, saturation exponent decreased, the main peak of NMR T_2 spectra moved to the left, and the pore volume of free fluid also decreased. Meanwhile, the location of MPMI curves moved upward.

Figure 6a–f displays the crossplots of saturation exponent versus pore structure parameters for all 18 core samples. These figures notably exhibited that the value of saturation exponent

Fig. 4 Relationships between cementation exponent and pore structure parameters for 18 core samples
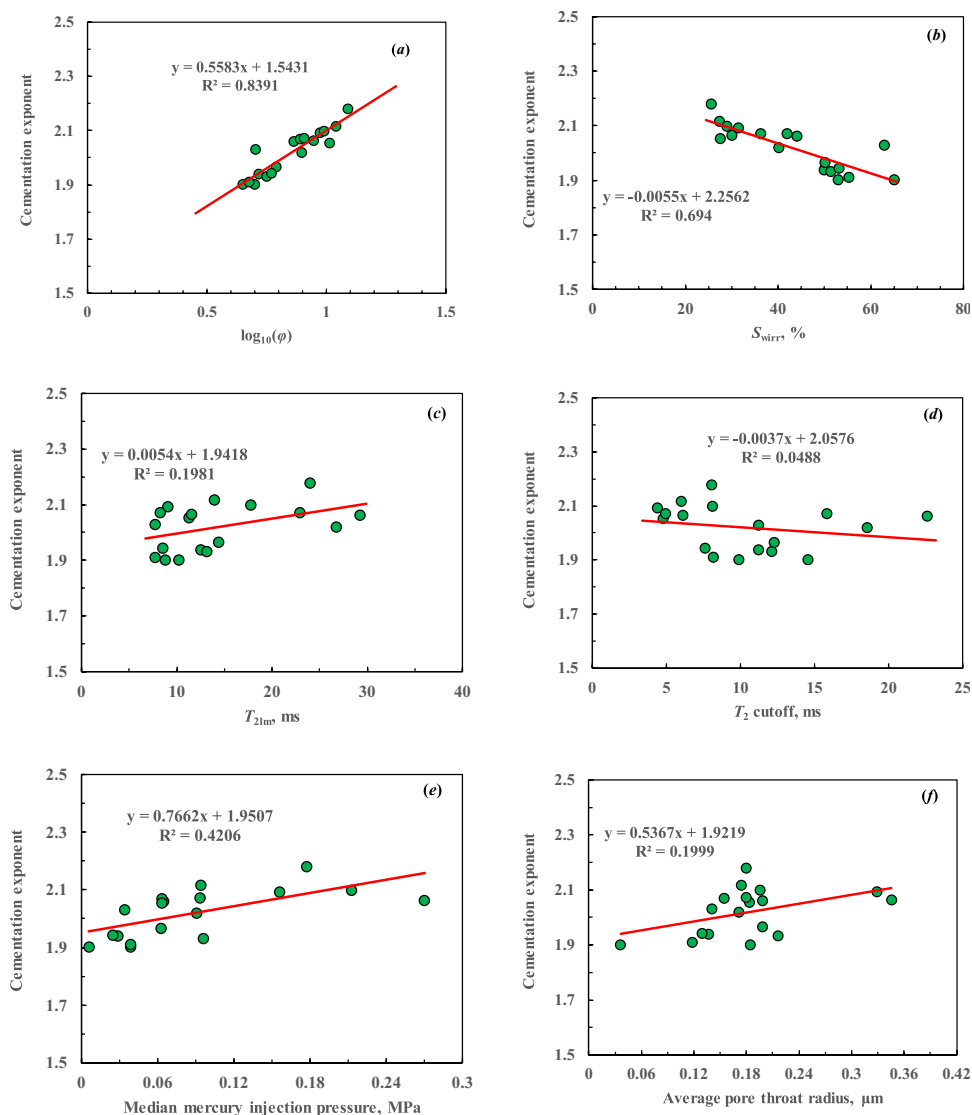
was inversely proportional to pore structure for our target tight sandstone reservoirs. Rocks with poor pore structure always contained relatively high saturation exponent, and vice versa. Hence, it was illogical to calculate water saturation by using fixed saturation exponent for all types of formations.

Models of predicting cementation exponent and saturation exponent from NMR logging

Establishment of cementation exponent and saturation exponent prediction models

Figures 4 and 6 clearly indicated that cementation exponent was associated with porosity and irreducible water saturation; whereas, saturation exponent was heavily affected by rock porosity and the ratio of large pore volume to small pore volume (defined by $(100-S_{wirr})/S_{wirr}$). Hence, to accurately predict water saturation, we chose porosity and irreducible water saturation as sensitive parameter to establish cementation exponent prediction model, and porosity $(100-S_{wirr})/S_{wirr}$ was chosen to calculate saturation exponent.

Using resistivity experimental results of 18 core samples as the data set, various cementation exponent and saturation exponent prediction models were established and listed:

$$m = 0.967 \times \log_{10}(\varphi) + 0.005 \times S_{wirr}, \; R^2 = 0.935, \quad (3)$$

$$n = 0.003 \times \varphi^2 - 0.027 \times \varphi - 0.155 \times \frac{100 - S_{wirr}}{S_{wirr}}, \; R^2 = 0.876, \quad (4)$$
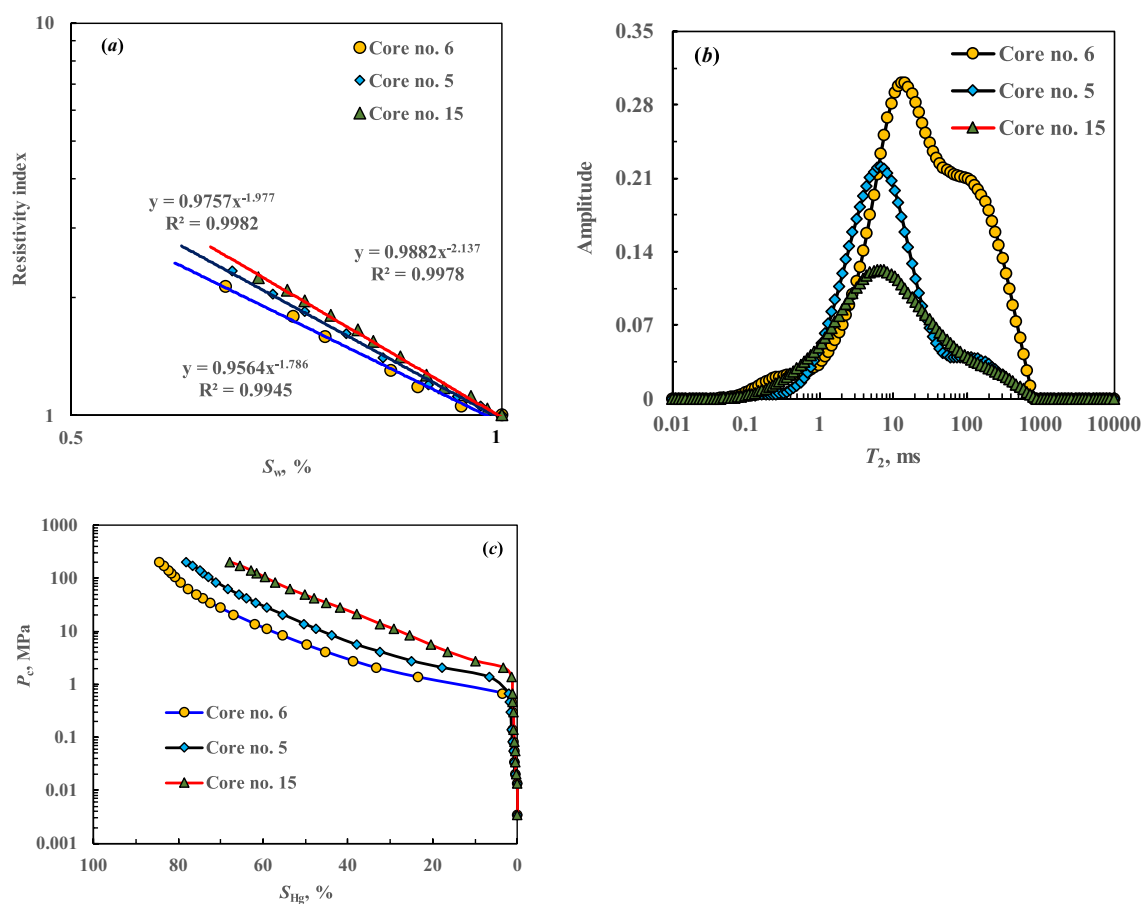
Fig. 5 Crossplot of water saturation versus resistivity index (**a**), NMR T_2 distributions (**b**) and HPMI curves (**c**) for three typical core samples

where S_{wirr} was the irreducible water saturation in %.

To use Eqs. 3 and 4 to calculate cementation exponent and saturation exponent, porosity and S_{wirr} should be first acquired. Porosity can be easily accurately calculated by combining with NMR and conventional logging, e.g., density or acoustic logging (Freedman et al. 1998; Abu-Shanab et al. 2005; Jain et al. 2019). However, S_{wirr} calculation was heavily depended on T_2 cutoff. Xiao et al. (2018) pointed out that various T_2 cutoff should be used to calculate S_{wirr} in heterogeneous formation. However, the number of core samples was not enough, and T_2 cutoff distribution for 18 core samples was relatively concentrated (Fig. 7). Hence, we used unified T_2 cutoff (defined as the average value of T_2 cutoff for all core samples) to calculate S_{wirr}. In our study, the average T_2 cutoff for 18 core samples was 10.38 ms. Hence, it was used to calculate S_{wirr} from NMR logging by using Eq. 5:

$$S_{wirr} = \frac{\int_{T_{2,min}}^{10.38} S(T)dt}{\int_{T_{2,min}}^{T_{2,max}} S(T)dt}, \tag{5}$$

where $T_{2,min}$ and $T_{2,max}$ were the minimal and maximal transverse relaxation time, separately, and their unit was ms. $S(T)$ was a function that associated with transverse relaxation time.

Reliability verification

To verify the reliability of Eqs. 3 and 4, we extended them into field applications to process NMR logging data in wells A and B. Consecutive cementation exponent and saturation exponent curves were predicted. We extracted cementation exponent and saturation exponent that corresponded to the depths of core samples. In Fig. 8a and b, we compared predicted cementation exponent and
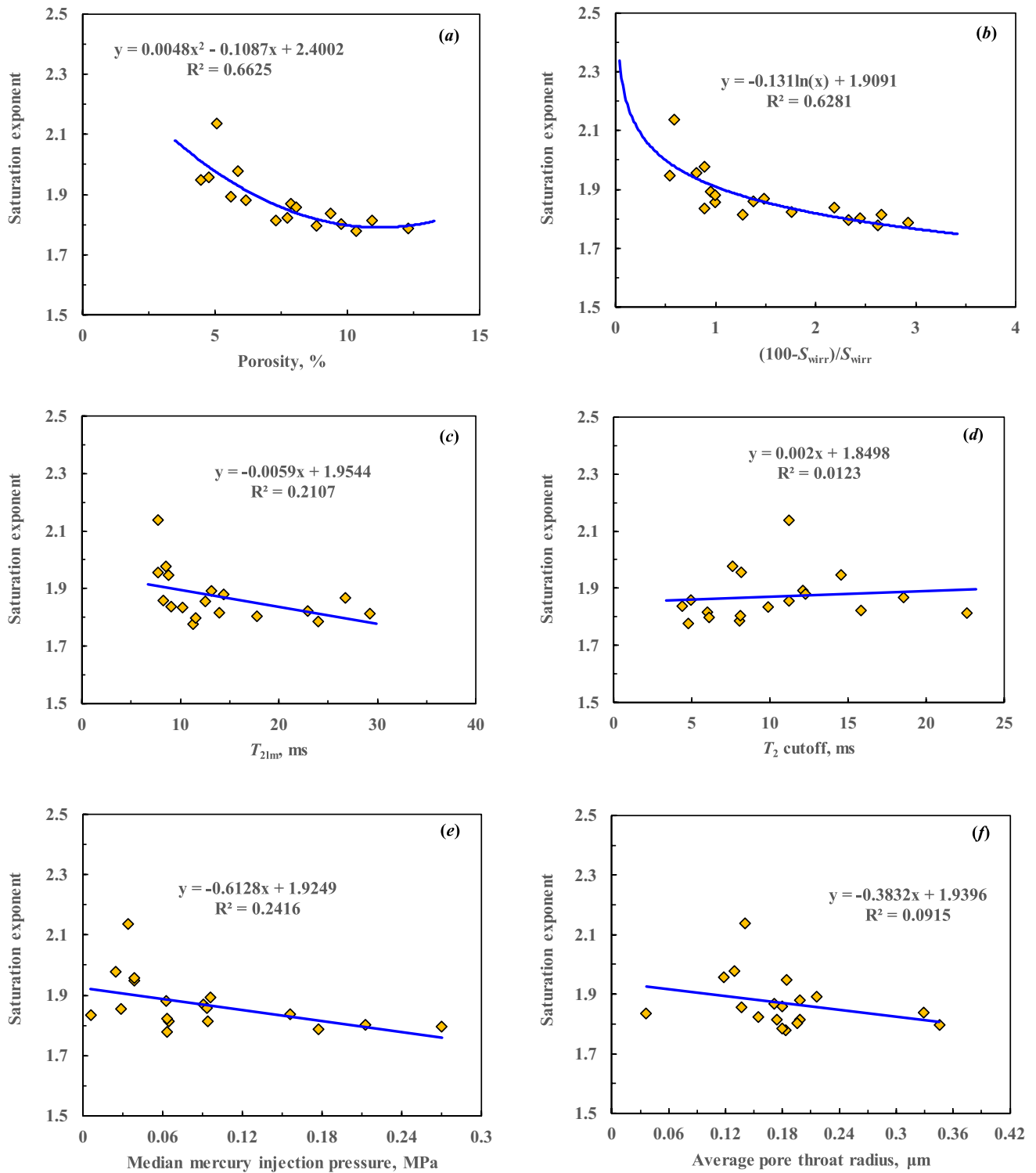
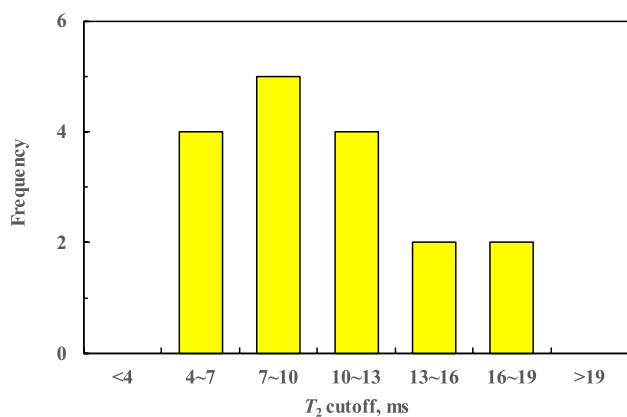**Fig. 6** Relationships between saturation exponent and pore structure parameters for 18 core samples

Fig. 7 Statistical histogram of T_2 cutoff for all 18 core samples. The average T_2 cutoff was 10.38 ms, and it was defined as the optimal T_2 cutoff to calculate S_{wirr} from NMR logging

Case studies

By using our raised models, several wells, which located in northwestern Sichuan Basin, were processed to acquire cementation exponent and saturation exponent curves from NMR logging, and they were substituted into Archie's equation to optimize saturation estimation model. We consecutively predicted water saturation curves by using optimized Archie's equation. To verify the superiority of our optimized models, we also calculated water saturation by using classic Archie's equation, and the used rock resistivity parameters are fixed and extracted from Fig. 1. Figure 9 displays the comparison of predicted water saturations based on two different types of methods with core-derived results in one well. In this figure, conventional well logging curves were displayed in the first three tracks, and they were used to indicate effective reservoir, calculate porosity, and identify pore fluids, separately. In the fourth track, we displayed NMR T_2 spectra (T2_DIST), which were acquired from Schlumberger's CMR-Plus tool. The T_2 spectra exhibited as typical bimodal to multimodal distribution, indicating complicated pore structure in our target tight sandstone reservoir. In the fifth and sixth tracks, formation porosity (POR) and permeability (PERM) were displayed, separately. They clearly indicated that formation porosity was lower than 14.0%, and permeability was lower than 1.0 mD. Comparisons of predicted cementation exponent (m) and saturation exponent (n) with core-derived results (Core_m and Core_n) were displayed in the seventh and eighth tracks, respectively. Good consistency between these two types of resistivity parameters illustrated that our raised models were reliable. In the ninth track, we compared predicted water saturations with core-derived results. In this track, Sw_Archie represented the calculated

saturation exponent from field NMR logging with core-derived results, separately. The red dotted lines in these two figures were the 45^0 diagonal lines, they were used to indicate the consistency between two types of data points. These two figures clearly indicated that the data points evenly distributed around diagonal lines, these meant that predicted cementation exponent and saturation exponent were all accurate. Further quantitative analysis showed that the absolute errors between predicted cementation exponent and core-derived results were lower than 0.05; whereas, the absolute errors between predicted saturation exponent and core-derived results can be controlled within ± 0.07. These absolute errors were low enough for water saturation estimation (Xiao et al. 2013).
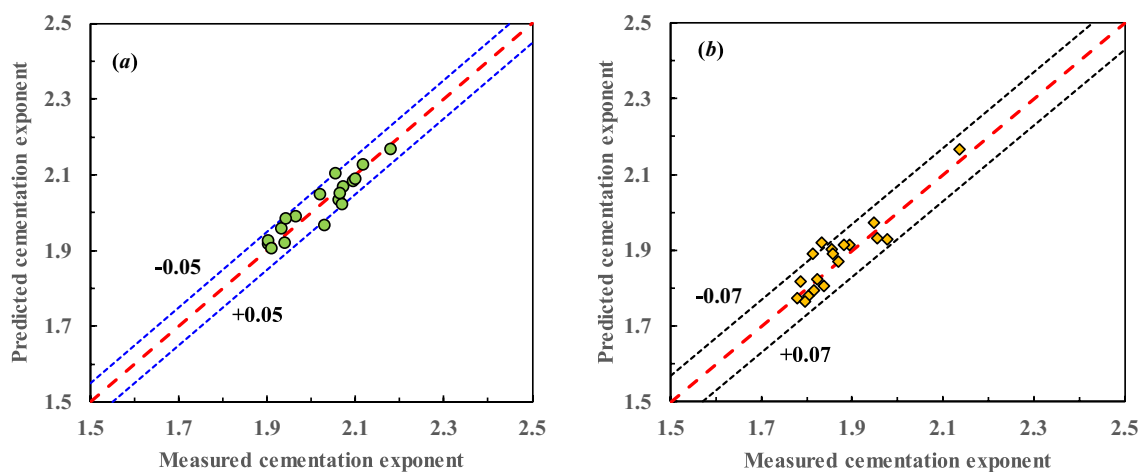

Fig. 8 Comparisons of measured cementation exponent (**a**) and saturation exponent (**b**) in laboratory with predicted results based on our raised optimized models
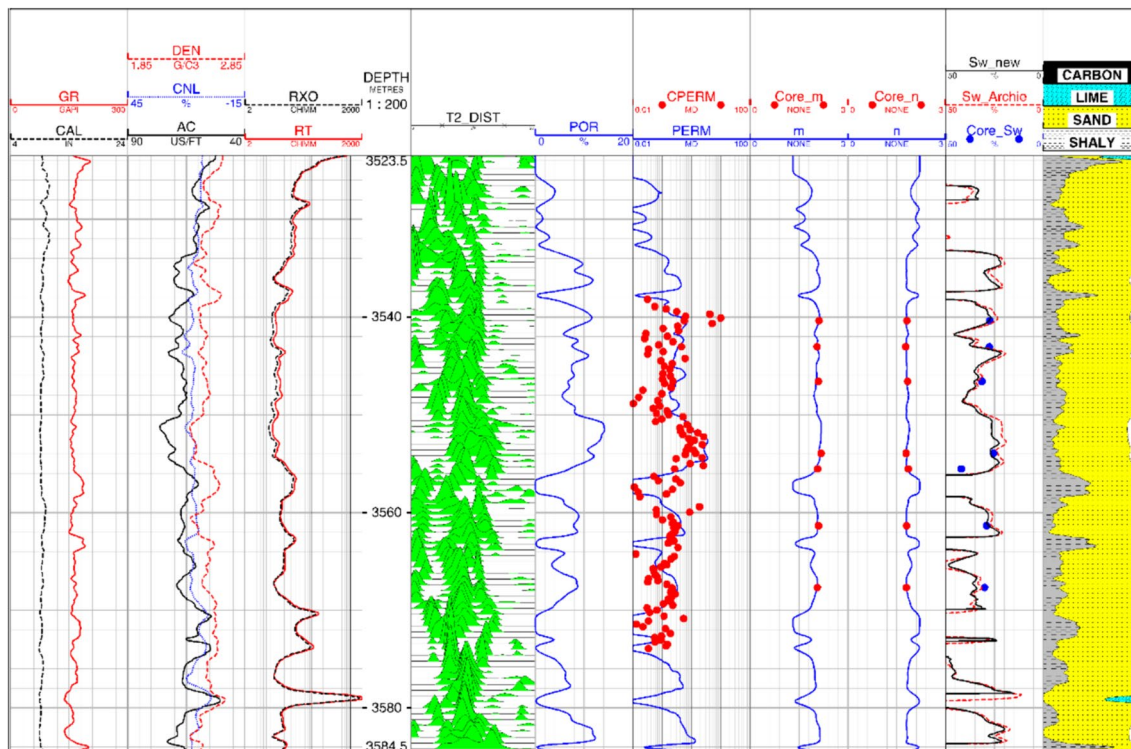
Fig. 9 Comparisons of predicted water saturations by using two methods with core-derived results in a well
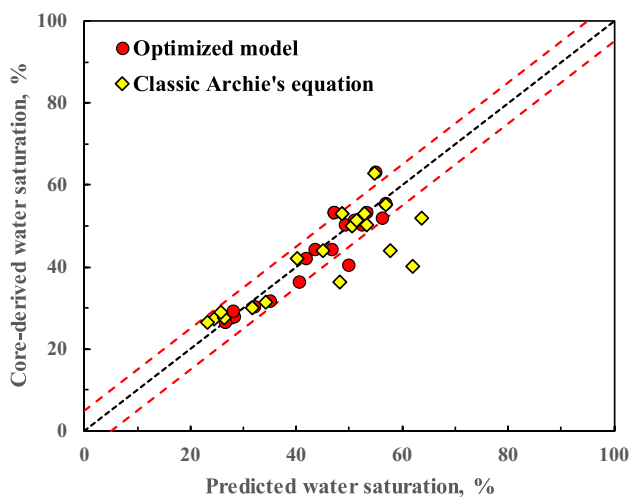

Fig. 10 Comparisons of predicted water saturations based on two methods and core-derived results in our target tight gas sandstone reservoirs

water saturation based on classic Archie's equation, and used resistivity parameters were fixed. Sw_new was the predicted water saturation by using optimized Archie's equation based on our raised models in this study; whereas, Core_Sw was core-derived water saturation, it represented the true value in our target formation. Comparisons illustrated that predicted water saturation based on our raised optimized

models matched well with core-derived water saturation. Whereas calculated water saturation by using fixed resistivity parameters was all 3.0–5.0% lower than true water saturation. Our raised saturation optimized models were valuable in improving tight gas sandstone reservoirs characterization and reserve prediction.

To quantize the accuracy of predicted water saturations by using two methods, we extracted calculated water saturation that corresponded to the depth of core samples. Figure 10 exhibits the crossplot of calculated water saturations by using classic Archie's equation, optimized models, separately and core-derived results. The black dashed line was a 45° diagonal, it was used to quantize the accuracy. The red dotted lines were the ±5% margin of error. This figure notably indicated that the predicted water saturations by using optimized models were close to core-derived results, and the absolute errors between them were lower than 5%. However, if we directly calculated water saturations by using classic Archie's equation, they would be overestimated.

Conclusions

Water saturation estimation in tight gas sandstone reservoir was difficult by directly using classic Archie's equation due to the effect of complicated pore structure. The resistivity parameters were heavily affected, this made crossplots of

porosity and formation factor, water saturation versus resistivity index were divergent, and inaccurate water saturation should be calculated unless the input parameters were optimized.

Experimental results of 18 typical core samples illustrated that pore structure was directly proportional to cementation exponent, and inversely proportional to saturation exponent. This was to say, formations with better pore structure always contained high cementation and lower saturation exponent. Two parameters, which were porosity and irreducible water saturation, were sensitive to cementation exponent, and porosity and ratio of large pore volume to small pore volume ($(100-S_{wirr})/S_{wirr}$)) were associated with saturation exponent. Two optimized models, which were used to calculate various cementation exponent and saturation exponent from NMR logging, were raised.

Field applications illustrated that the optimized models were valuable in predicting cementation exponent and saturation exponent. The absolute errors of them were lower than 0.05 and 0.07, separately. After optimized resistivity parameters were substituted into classic Archie's equation, reasonable water saturation was precisely calculated; whereas, the predicted water saturation by using fixed resistivity parameters were overestimated.

Author contributions Xiaoyong Xia was involved in funding acquisition, processing NMR logging and writing original draft. Bing Han was involved in applying for the resistivity and HPMI experiments. Bing Xie was involved in processing field NMR logging and analyzing the accuracy. Qiang Lai was involved in applying for the NMR experiment in laboratory. Yuexiang Wang was involved in establishing the optimized water saturation estimation models. Shaowu Zhu was involved in raising the technique and revising the draft.

Declarations

Conflict of interest The authors declare no conflict of interest.

References

Abu-Shanab MM, Hamada GM, El Oraby M (2005) DMR technique improves tight gas porosity estimate. Oil Gas J 103(47):54–57

Ahmed AS, Revil A, Byrdina S, Coperey A, Gailler L, Grobbe N, Viveiros F, Silva C, Jougnot D, Ghorbani A, Hogg C, Kiyan D, Rath V, Heap MJ, Grandis H, Humaida H (2018) 3D electrical conductivity tomography of volcanoes. J Volcanol Geoth Res 356:243–263. https://doi.org/10.1016/j.jvolgeores.2018.03.017

Ammar AI (2021) Development of numerical model for simulating resistivity and hydroelectric properties of fractured rock aquifers. J Appl Geophys 189:104319. https://doi.org/10.1016/j.jappgeo.2021.104319

Archie GE (1942) The electrical resistivity log as an aid in determining some reservoir characteristics. Trans AIME 146:54–62

Clavier C, Coates G, Dumanoir J (1984) Theoretical and experimental bases for the dual-water model for interpretation of shaly sands. SPE J 24(2):153–168. https://doi.org/10.2118/6859-PA

Coates GR, Xiao LZ, Prammer MG (2000) NMR logging principles and applications: Houston. Gulf Publishing Company, Texas, pp 1–256

Dunn KJ, Bergman DJ, Latorraca GA (2002) Nuclear magnetic resonance: petrophysical and logging applications. Handbook of geophysical exploration: seismic exploration, New York, Pergamon, vol 32, pp 1-293

Ferraris P, Carnegie AJ (2005) Integrated downhole fluid-identification applications for complex reservoir development. In: Proceeding of SPE Latin American and Caribbean petroleum engineering conference. https://doi.org/10.2118/94860-MS

Freedman R, Minh CC, Gubelin G, Freeman JJ, McGinness T, Terry B, Rawlence D (1998) Combining NMR and density logs for petrophysical analysis in gas-bearing formations. In: SPWLA 39th annual logging symposium

Gao FM, Xiao L, Zhang W, Cui WP, Zhang ZQ, Yang EH (2023) Low permeability gas-bearing sandstone reservoirs characterization from geophysical well logging data: a case study of Pinghu formation in KQT Region. East China Sea Processes 11(4):1030. https://doi.org/10.3390/pr11041030

Givens WW (1987) A conductive rock matrix model (CRMM) for the analysis of low-contrast resistivity formations. Log Analyst 28(2):138–151

Givens WW, Schmidt EJ (1988) A generic electrical conduction model for low-contrast resistivity sandstones. In: SPWLA 29th annual logging symposium

Guo LX, Ma GW, Chen GQ (2023) A micro frost heave model for porous rock considering pore characteristics and water saturation. Comput Geotech 166:106029. https://doi.org/10.1016/j.compgeo.2023.106029

Gupta AR, Kamal (2023) A theoretical approach for water saturation estimation in shaly sandstones. Geoenergy Sci Eng 228:212001. https://doi.org/10.1016/j.geoen.2023.212001

Hou YT, Liu D, Zhao TP, Zhou JY, Tian LL, Kou XP, Zhu BD, Nie X (2023) Numerical simulation of electrical properties of carbonate reservoirs using digital rocks. Processes 11(7):2214. https://doi.org/10.3390/pr11072214

Jain V, Saumya S, Vij J, Singh J, Singh B, Pattnaik S, Oli A, Kumar P, Collett TS (2019) New technique for accurate porosity estimation from logging-while-drilling nuclear magnetic resonance data, NGHP-02 expedition, offshore, India. Mar Pet Geol 108:570–580. https://doi.org/10.1016/j.marpetgeo.2018.11.001

Li X, Zhao WZ, Zhou CC, Wang TS, Li CL (2012) Dual-porosity saturation model of low-porosity and low-permeability clastic reservoirs. Pet Explor Dev 39(1):88–98. https://doi.org/10.1016/S1876-3804(12)60019-6

Li X, Li CL, Li B, Liu XF, Yuan C (2020) Response laws of rock electrical property and saturation evaluation method of tight sandstone. Pet Explor Dev 47(1):214–224. https://doi.org/10.1016/S1876-3804(20)60020-9

Li JQ, Xiao XH, Chi RQ, Wen HC, Zhang WJ (2023) Formation characterization and type prediction based on geophysical well log data in horizontal well: a case study of Triassic Chang 8 formation in shunning region. Central Ordos Basin Processes 11(8):2297. https://doi.org/10.3390/pr11082297

Liu XF, Sun JM, Wang HT (2009) Numerical simulation of rock electrical properties based on digital cores. Appl Geophys 6(1):1–7. https://doi.org/10.1007/s11770-009-0001-6

Liu XP, Hu XX (2010) A novel method to identify pore fluid in low porosity/low permeability gas zones. In: Proceeding of SPE Latin

American and Caribbean petroleum engineering conference. https://doi.org/10.2118/118970-MS

Liu XP, Hu XX, Xiao L (2012) Effects of pore structure to electrical properties in tight gas reservoirs: an experimental study. In: Proceeding of SPE/EAGE European unconventional resources conference and exhibition. https://doi.org/10.2118/150926-MS

Mahmood A, Aboelkhair H, Attia A (2023) Investigation of the effect of tortuosity, hydrocarbon saturation and porosity on enhancing reservoir characterization. Geoenergy Sci Eng 227:211855. https://doi.org/10.1016/j.geoen.2023.211855

Mao ZQ, Tan TD, Lin CZ, Wang Q (1997) The laboratory studies on pore structure and electrical properties of core samples fully-saturated with brine water. Acta Petrolei Sinica 18(3):51–55. https://doi.org/10.7623/syxb199703008

Mao ZQ, Gong FH, Liu CY, Zhu DC, Zuo ZG (1999) Experimental study on the gensis of low resistivity pay zone in north Region of Tarim Basin (I). Well Logging Technol 23(4):243–245

Mao ZQ, Xiao L, Wang ZN, Jin Y, Liu XG, Xie B (2013) Estimation of permeability by integrating nuclear magnetic resonance (NMR) logs with mercury injection capillary pressure (MICP) data in tight gas sands. Appl Magn Reson 44(4):449–468. https://doi.org/10.1007/s00723-012-0384-z

Mo XW, He DH, Li ZB, Wen XC, Li GR (2001) The application of three-water conduction model in the interpretation of low-resistivity reservoir. J Jilin Univ: Earth Sci Edition 31(1):92–95

Picket GR (1966) A review of current techniques for determination of water saturation from logs. J Petrol Technol 18(11):1425–1433. https://doi.org/10.2118/1446-PA

Poupon A, Leveaux J (1971) Evaluation of water saturation in shaly formations. In: SPWLA 12th annual logging symposium

Qian C, Li XZ, Zhang Q, Shen WJ, Guo W, Lin W, Han LL, Cui Y, Huang YZ, Pei XY, Yu ZC (2023) Reservoir characteristics of different shale lithofacies and their effects on the gas content of Wufeng–Longmaxi formation, southern Sichuan Basin. China Geoenergy Sci Eng 225:211701. https://doi.org/10.1016/j.geoen.2023.211701

Rasmus JC (1985) A summary of the effects of various pore geometrics and their wettabilities on measured and in-situ values of cementation and saturation exponents. Petrophysics 28(2):152–164

Sarihi A, Vargas-Murillo B (2015) A method to compute water saturation in tight rocks accounting for conductivity of clay minerals. In: Proceeding of Abu Dhabi international petroleum exhibition and conference. https://doi.org/10.2118/177550-MS

Simandoux P (1963) Dielectric measurements on porous media and application to the measurements of watersaturation: study of behavior of argillaceous formations. Revue De L'instiut Francese Du Petrol 18:193–215

Song YJ, Wang Q, Yin CH (1995) A new S-B conductivity model for determining water saturation of shaly sands. Well Logging Technol 19(4):244–249

Umezawa R, Katsura M, Nakashima S (2021) Effect of water saturation on the electrical conductivity of microporous silica glass.

Transp Porous Media 138(1):225–243. https://doi.org/10.1007/s11242-021-01601-6

Walsh SDC, Vogler D (2020) Simulating electropulse fracture of granitic rock. Int J Rock Mech Min Sci 128:104238. https://doi.org/10.1016/j.ijrmms.2020.104238

Waxman MH, Smits LJM (1968) Electrical conductivities in oil-bearing shaly sands. Soc Petrol Eng J 8(2):107–122. https://doi.org/10.2118/1863-A

Waxman MH, Thomas EC (1974) Electrical conductivities in shaly sands—I. The relation between hydrocarbon saturation and resistivity index; II. The temperature coefficient of electrical conductivity. J Petroleum Technol 26(2):213–225. https://doi.org/10.2118/4094-PA

Waxman MH, Thomas EC (2007) Technical Note: An addendum to electrical conductivities in shaly sands—I. The relation between hydrocarbon saturation and resistivity index; II. The temperature coefficient of electrical conductivity. SPE J 12(4):392. https://doi.org/10.2118/109632-PA

Xiao L, Zou CC, Mao ZQ, Shi YJ, Liu XP, Jin Y, Guo HP, Hu XX (2013) Estimation of water saturation from nuclear magnetic resonance (NMR) and conventional logs in low permeability sandstone reservoirs. J Petrol Sci Eng 108:40–51. https://doi.org/10.1016/j.petrol.2013.05.009

Xiao L, Mao ZQ, Jin Y (2015) Tight gas sandstone reservoirs evaluation from nuclear magnetic resonance (NMR) logs: case studies. Arab J Sci Eng 40(4):1223–1237. https://doi.org/10.1007/s13369-015-1608-y

Xiao L, Mao ZQ, Zou CC, Jin Y, Zhu JC (2016) A new methodology of constructing pseudo capillary pressure (Pc) curves from nuclear magnetic resonance (NMR) logs. J Petrol Sci Eng 147:154–167. https://doi.org/10.1016/j.petrol.2016.05.015

Xiao L, Li JR, Mao ZQ, Lu J, Yu HY, Guo HP, Li GR (2018) A method to determine nuclear magnetic resonance (NMR) T2cutoff based on normal distribution simulation in tight sandstone reservoirs. Fuel 225:472–482. https://doi.org/10.1016/j.fuel.2018.03.178

Xie WB, Yin QL, Zeng JB, Wang GW, Feng C, Zhang P (2023) Fractal-based approaches to pore structure investigation and water saturation prediction from NMR measurements: a case study of the gas-bearing tight sandstone reservoir in Nanpu Sag. Fractal Fract 7(3):273. https://doi.org/10.3390/fractalfract7030273

Zhang LH, Pan BZ, Li ZB, Mo XW, Xia ZL, Xu WL (2010) New three water conduction model and its application in the evaluation of low porosity and low permeability reservoir. Petroleum Geophys Prospect 45(3):431–435